Geophysical Research Letters

RESEARCH LETTER
10.1029/2018GL079027

Key Points:
- Recent *M*~4 induced earthquakes in western Canada can be categorized into strike-slip and reverse-faulting regimes, similar to tectonic ones
- Consistent CLVD components reflect fault/fracture growth or en echelon fault slipping
- Induced earthquakes exhibit indistinguishable amounts of non-DC components from tectonic earthquakes

Supporting Information:
- Supporting Information S1
- Data Set S1

Correspondence to:
R. Wang,
ruijia.wang@ualberta.ca

Citation:
Wang, R., Gu, Y. J., Schultz, R., & Chen, Y. (2018). Faults and non-double-couple components for induced earthquakes. *Geophysical Research Letters*, *45*. https://doi.org/10.1029/2018GL079027

Received 11 JUN 2018
Accepted 28 JUL 2018
Accepted article online 6 AUG 2018

Faults and Non-Double-Couple Components for Induced Earthquakes

Ruijia Wang[1], Yu Jeffrey Gu[1], Ryan Schultz[2], and Yunfeng Chen[1]

[1]Department of Physics, University of Alberta, Edmonton, Alberta, Canada, [2]Alberta Geological Survey, Alberta Energy Regulator, Edmonton, Alberta, Canada

Abstract Focal mechanisms of induced earthquakes reflect anthropogenic contributions to preexisting geological features and fault slippages. In this paper, we examine fault-related (double-couple (DC)) and possibly fluid-related (non-double-couple (non-DC)) mechanisms of induced earthquakes (*M*2–6) at regional scales. We systematically compare well-resolved focal mechanisms of 33 events in the Western Canada Sedimentary Basin, among which 12 were induced by hydraulic fracturing and one by secondary recovery. Most of the seismicity is dominated by strike-slip/thrust faulting regimes, whereas limited (but consistent) non-DC components are obtained from injection-induced seismicity in central Alberta. We interpret the persistent compensated-linear-vector-dipole components (*M*2.1–3.8) as reflecting fracture growth and/or noncoplanar faults slippages during hydraulic-fracturing stimulations. We further expand the moment tensor decomposition analysis to four representative classes of induced seismicity globally and find that the overall contribution of non-DC components is comparable between induced and tectonic earthquakes.

Plain Language Summary Source mechanism of induced (man-made) earthquakes reflects human contributions to the fault slippages. We examine fault-related and possibly fluid-related components of the earthquake sources from western Canada and find evidence for fracture growth and/or nonplanar fault slippages during hydraulic-fracturing stimulations. We also systematically compare the well-resolved focal mechanisms of 79 earthquakes (induced by different reasons) with 24 natural ones. The results of our statistical analysis suggest that induced and natural earthquakes are similar in view of source mechanism.

1. Introduction

In recent years, increases of seismicity rate induced by industrial activities (e.g., McGarr et al., 2015) have invited both critical scientific inquiries and public scrutiny due to its potential impact on seismic hazard assessment (Mignan et al., 2017; Petersen et al., 2017; Schultz et al., 2018). Induced earthquakes large enough to be felt have been widely reported in the United States (Ellsworth, 2013), Canada (Bao & Eaton, 2016), Germany (Evans et al., 2012), South Korea (Grigoli et al., 2018; Kim et al., 2018), and other countries (see Foulger et al., 2018 and Grigoli et al., 2017 for detailed reviews). Their relationships with fluid injection have been explained both conceptually (Doglioni, 2017; Ellsworth, 2013; Schmitt, 2014) and physically through geomechanical modeling (e.g., Zhang et al., 2013), laboratory experiments (e.g., Guglielmi et al., 2015), and multiscale observations (e.g., Dahm et al., 2013; McGarr & Barbour, 2017).

Source/faulting properties are commonly resolved to identify, evaluate, and manage induced earthquakes. In many cases, focal mechanism solutions are used to infer the orientation and stress condition surrounding (often unmapped) reactivated faults. The double-couple (DC) component therein directly reflects the size and orientation of the reactivated fault and are generally well constrained in induced seismogenic zones (e.g., western Canada (Wang et al., 2017); Oklahoma, USA (Chen et al., 2017; Schoenball et al., 2018)). The non-DC components reflect fault or fracture growth due to possible volume changes associated with fluid injection/extraction. While a few recent studies (e.g., Cesca et al., 2013; Zhang et al., 2016; Zhao et al., 2014) quantified the amount of non-DC components of induced events, characterizing and virtualizing non-DC components, especially those pertaining to fluid-injection induced earthquakes at the regional scale, remains a work in progress.

Among the various challenges, insufficient station density near focal zones and low accuracy in averaged (often one-dimensional) regional structural models are the most glaring issues in assessing the non-DC

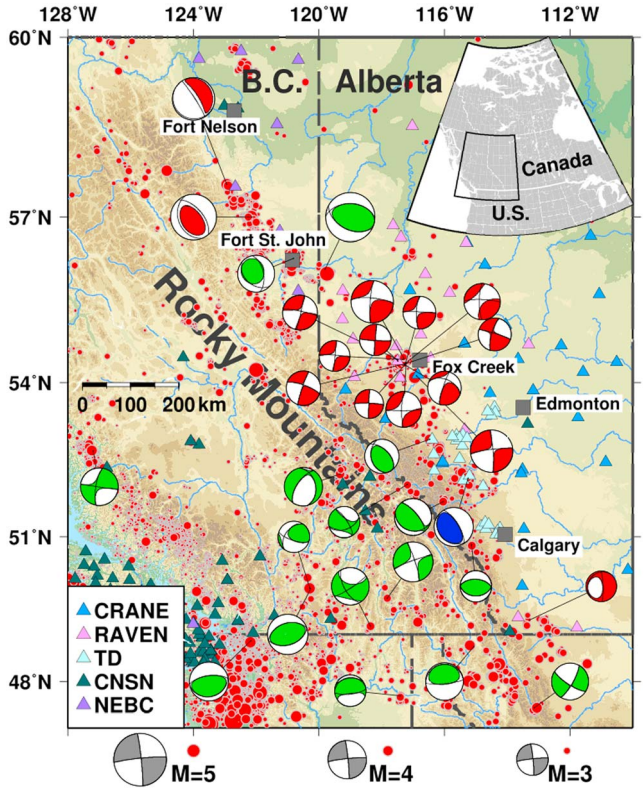

Figure 1. Distribution of stations (triangles) and earthquakes (small red circles) in western Canada (1985–2017). The magnitude-scaled "beach balls" show the focal mechanisms of tectonic (green), hydraulic-fracturing-induced (red), and secondary-recovery-induced (blue) events.

contributions to fluid-induced events (e.g., Wang et al., 2016; Zhang et al., 2016). In this paper, we simultaneously decipher the DC and non-DC components in the source analyses of regional seismic events. Our targets are shallow (depth $<$ 10 km) intraplate earthquakes in western Canada—a region where most induced seismicity is caused by hydraulic fracturing (Atkinson et al., 2016). This study presents the detailed characteristics of DC and non-DC components from well-resolved full moment tensors of induced events (2013–2017) and shallow intraplate tectonic earthquakes (1985–2007). We extend this analysis to the global scale based on four representative induced seismicity clusters (103 events) where full moment tensor solutions are available.

2. Background and Data Sets

2.1. Recent Intraplate Events in Western Canada

The Western Canada Sedimentary Basin (WCSB) had been a seismically quiescent region historically. Only one known $M > 5$ earthquake (M5.1 in 2001) was cataloged as a natural event occurring under presumed influences of regional tectonic forces. However, regional seismic rate has increased exponentially since 2010, during which several felt earthquakes were reported (van der Baan & Calixto, 2017) and linked to wastewater disposal (Schultz et al., 2014) or hydraulic fracturing (Atkinson et al., 2016). The largest induced earthquake occurred in 2015 in northern British Columbia, reaching a moment magnitude of 4.6 (Babaie Mahani et al., 2017) while others clustered near central (e.g., Fox Creek; Schultz et al., 2017; Wang et al., 2016, 2017) and southern (Schultz et al., 2015) Alberta. Events in central Alberta are induced by different wells with separation distances as large as 40 km over a period of 4 years. Based on regional seismic monitoring, no $M_L > 4$ (local magnitude) events were reported in 2017, but the total number of $M_L > 3$ events (72) surpassed that of previous years (Earthquakes Canada, 2018).

Distinct from the scattered natural events near the Canadian Rockies, the locations of recent earthquakes are inundated by industrial operations (Figure 1). Induced events form tight clusters within kilometers of suspected injection sites, which largely target two shale-gas formations: the Montney in northern British Columbia and the Duvernay in central-southern Alberta. The potential faults associated with recent clusters are smaller than, and away from, major thrust fault systems within the Canadian Rockies. Most of the events fall below the magnitude threshold of automatic moment tensor inversion and require a case-by-case analysis to delineate the reactivated fault geometry. By exploiting the expanding regional seismic networks, we systematically resolved the full moment tensors for M3–4 events and provided more reliable assessments of the non-DC components.

2.2. Representative Worldwide Cases

Globally, there have been more than 700 industrial sites with reported or suggested induced earthquakes, 88% of which are attributable to mining, wastewater disposal, oil/gas exploration, and geothermal exploitation (Foulger et al., 2018; Wilson et al., 2017). The largest magnitudes of most induced earthquakes are smaller than 2—below the threshold of reliable full moment tensor retrievals based on regional networks largely designed for natural earthquake hazard monitoring. On the other end of the spectrum, the causes of some devastating earthquakes ($M > 7$; e.g., the Wenchuan earthquake) are under debate as either natural or partially induced (Ge et al., 2009; Tao et al., 2015) and may not represent induced earthquakes with dominating anthropogenic contributions (if any). These debatable cases of seismicity are also excluded from our moment tensor decomposition in section 3.

To compare our WCSB events against induced earthquakes worldwide, we collected full moment tensors for events caused by (1) wastewater disposal in the central United States (see supporting information; also see

Huang et al., 2017 for the main catalog); (2) mining activity in and around Germany (Cesca et al., 2013); (3) multistage hydraulic-fracturing stimulation in the Sichuan Basin, China (Lei et al., 2013, 2017); and (4) geothermal exploitation in California, USA (Guilhem et al., 2014; Martínez-Garzón et al., 2017). In addition, tectonic earthquakes in central United States are included as a reference group to explore the potential differences between induced and natural earthquakes. All presented data sets share the common magnitude range of *M*3–6 (see Figure S4 in the supporting information) to avoid potential mechanism differences between microseismic and regional-scale earthquakes.

3. Moment Tensors Solutions and Decomposition

The expanding seismic network in the WCSB (Schultz & Stern, 2015) enables possible determinations of moment tensors for events as small as *M*3. To do so, we adopt a refined regional crustal model (see Figure S1) with location-based adjustments in the sedimentary layers (e.g., thinner for events further away from the mountain belt). During the time domain full moment tensor inversion, the displacement waveforms are filtered by 0.05–0.1, 0.08–0.4, and 0.4–0.9 Hz. The lowest-frequency range is processed with a weight of five (compare to one for the high-frequency ranges) to ensure a similar contribution (i.e., peak amplitude) during the inversion procedure. For near-source stations, both frequency ranges contain all phases (body and surface waves), whereas only first arrivals (mainly body waves) from high frequencies at far-field stations ($>$100 km) are fitted. For shallow earthquakes, a multifrequency joint inversion approach (as adopted by our study) helps to reduce the potential trade-off between the non-DC components and focal depth. The variance reduction (VR) and decomposed results are summarized in Data set S1. To assess the stability of fault plane orientations, we perform a bootstrap resampling test (Efron & Tibshirani, 1991) 200 times on randomly formed subsets containing ~70% of the original seismograms (Figure 2a) for events recorded by more than eight stations. Although other smaller events are recorded by fewer stations, synthetic tests conducted under a four-station scenario (see supporting information) indicate that the challenges in obtaining reliable moment tensor solutions are not insurmountable (Fischer & Guest, 2011; Johnson et al., 2016; Pakzad et al., 2018; Šílený, 2009). On the one hand, our preferred source location and velocity model show strong tolerance to noise level (Figure 2b) during synthetic tests with limited station coverage: consistent focal solutions containing positive compensated-linear-vector-dipoles (CLVDs) are resolved at all the noise levels despite their relatively large amounts (compare with an input of 20%) when five or more times of the recorded noise are introduced. On the other hand, our joint inversions recover the input non-DC mechanisms (with VR $>$ 80%) when ~10% perturbations are applied to in the velocity model. Questionable results (i.e., incorrect non-DC mechanism or VR $<$ 50%) are obtained when all velocities are increased/decreased by 20%, which are extreme cases that are beyond our analysis. Based on the test results, we subjectively choose a VR $>$ 70% as an indicator of reliable inversion outcomes for events in western Canada.

Our final data set contains 103 full moment tensors with 79 induced events (see Table S1 for data). The decomposition of these events follows the convention of DC, CLVD, and the isotropic components as uniquely isolatable (Figure S3). We also provide an alternative major/minor DC decomposition (Jost & Herrmann, 1989) for events with consistent non-DC components in the WCSB. These two decomposition approaches favor different physical causes for induced events, and the outcomes are discussed in section 4.2.

4. Moment Tensor Decompositions and Implications

4.1. Double-Couple Faulting in Western Canada

Prior to 2007, 17 intraplate focal mechanisms were reported in western Canada and all the related earthquakes occurred within the mountain belt (see Figure 1; Ristau et al., 2007). These mechanisms exhibit substantial variations in faulting regimes and strike orientations, partially due to the limited seismic station coverage before 2010 (Gu et al., 2011). In comparison, fault plane solutions for seven recent *M*~4 events in this study are more stable and vary by less than 2.2° (see Figure 2). The *p* axes are uniformly aligned along the NE-SW, consistent with the dominant crustal stress orientations in western Canada (Heidbach et al., 2016). Despite the differences in location, causes, and stabilities, focal mechanisms of events in western Canada mainly fall into two faulting categories: (1) thrust near the Canadian Rockies and (2) strike-slip elsewhere (see Figure 1).

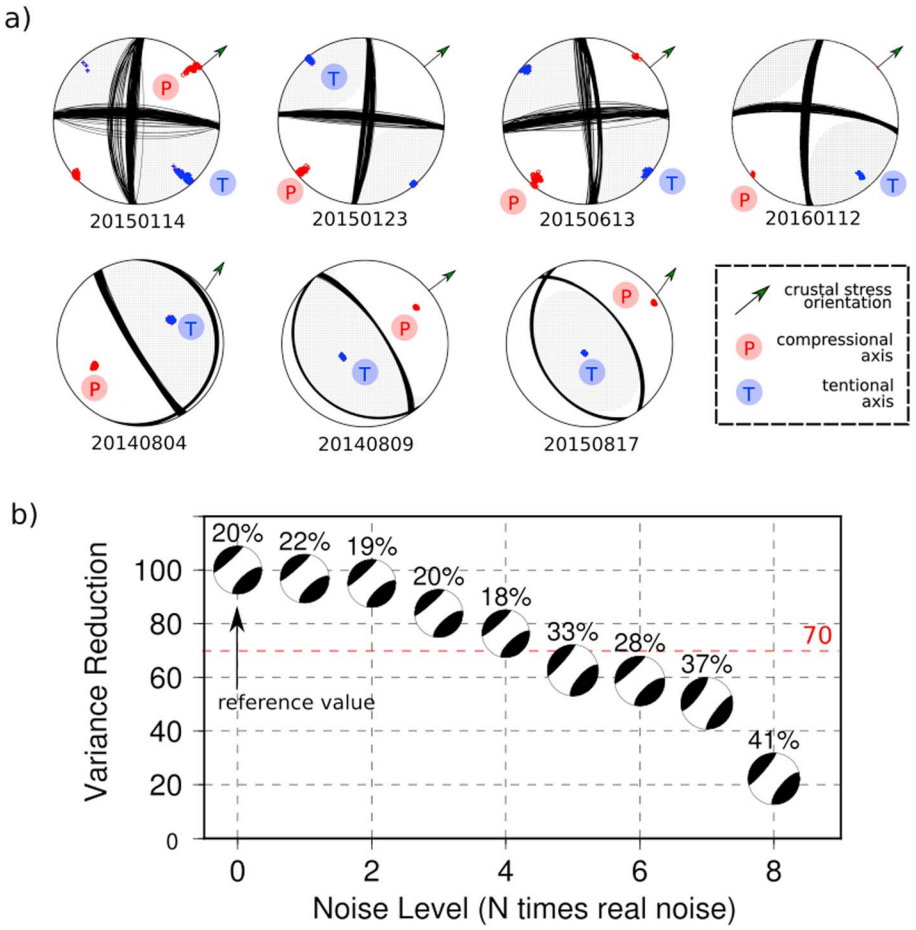

Figure 2. (a) Examples of fault plane solutions (uniform sizes) determined from bootstrap resampling test for events in the WCSB. The *p* axes are consistently aligned along NE-SW for both (top) strike-slip and (bottom) reverse-faulting mechanisms, comparable to nearby S_H orientation (Heidbach et al., 2016). (b) Variance reduction (fit) versus noise level during synthetic tests (see supporting information for detailed results and test on velocity model variation). Real noise is multiplied by *N* times and added to synthetic waveforms generated with 20% of CLVD and 0% of isotropic components. Only the non-DC components after decomposition are plotted and the corresponding percentages are labeled on top.

Both natural and induced events exhibit strike-slip-dominated faulting mechanisms basinward from the Canadian Rockies. Many of these induced events are associated with operations that hydraulically fractured the Duvernay formation (2.8–3.6-km depth; Dunn et al., 2012), which is within 1 km of the crystalline basement. Among the two candidate fault orientations (N-S or E-W), the existence of vertical N-S faulting system (within or above the basement) is supported by both geological and geophysical observations (Davies & Smith, 2006; Duggan et al., 2001; Schultz et al., 2016; Wang et al., 2017). At other locations, strike-slip-dominated tectonic events show similar fault plane orientations to those of induced events, with a lone outlier in western British Columbia (52.7°N, 127.2°W; see Figure 1) where complex crustal structures around Vancouver Island might be responsible (Ellis et al., 1983).

Along the Canadian Rockies, almost all events exhibit thrust-dominated faulting mechanisms. Natural events with thrust faulting slippages show variable strike orientations along E-W or NE-SW, including the *M*5.1 earthquake in 2001 (near Alberta and British Columbia border). An induced event in 2014 is located within northern British Columbia and shows either a near-vertical (84°) or a low-angle thrust fault (7°). The two remaining events with distinctive thrust components, that is, a secondary-recovery-induced event in central Alberta and a hydraulic-fracturing-induced case in northern British Columbia (see Figures 1 and 2), exhibit comparable (and moderate) dipping angles of 58° and 64°, respectively. The mechanisms of these two events are very similar to those of nearby (<100 km) tectonic earthquakes.

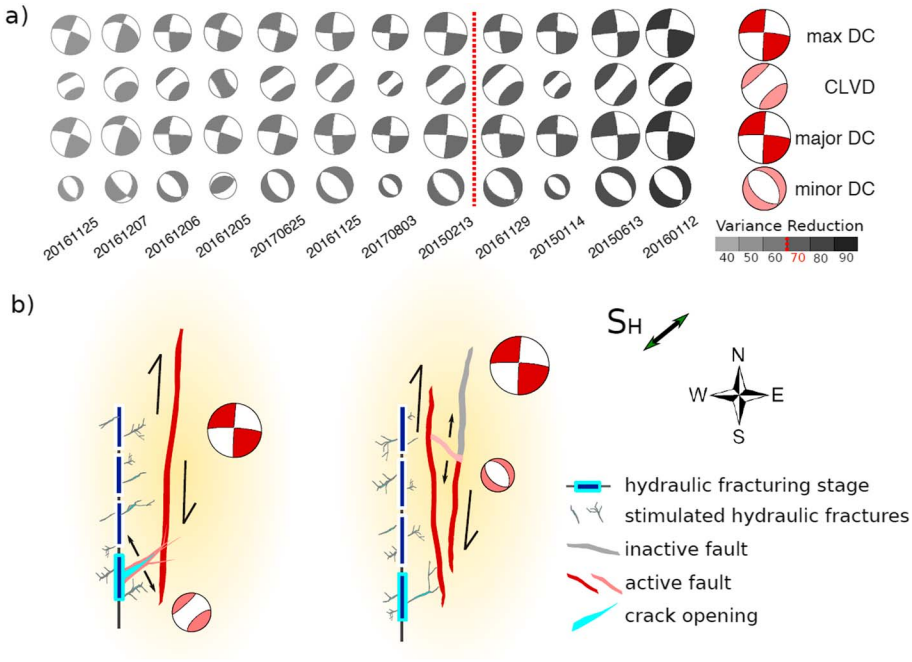

Figure 3. (a) Decomposition of the deviatoric parts for the hydraulic-fracturing-induced events in central Alberta. Event dates are indicated at the bottom and sizes of the different components are scaled to the magnitudes. These events are aligned by variance reduction values (see legend for the shade) and the red dashed line indicated 70% value. Normalized summations of each row are on the right. (b) Map view of the interpretations of the two decomposition styles related to hydraulic fracturing: (left) CLVD components and (right) minor DC components. Black arrows indicate relative motions. The minor fault (right) is extensional possibly due to the external pressure load on the highly fractured zone along the HF well.

For both strike-slip and thrust faulting regimes, the maximum horizontal stress (S_H) and vertical stress are the respective maximum stress magnitudes (Schmitt, 2014). Our *p* axis orientations from the focal mechanisms of recent earthquakes within the WCSB (see Figure 2) are predominantly along an NE-SW trend, which is consistent with the reported S_H direction in western Canada (Bell & Grasby, 2012; Reiter et al., 2014). The similarity between natural and induced DC components suggests that the strain release during an earthquake is dominated by the crustal stress condition and preexisting unmapped faults. This could manifest in induced earthquakes that are initiated by industrial activities, whereas the focal mechanisms are predominantly "preset" by the ambient stress condition and geology within the crust.

4.2. Interpretations of Non-Double-Couple Components

Despite known challenges in constraining non-DC components, we observe consistent CLVD motions from the strike-slip-dominated events in central Alberta (Figure 3a). We decompose the deviatoric part of a moment tenser in two ways: (1) DC and CLVD and (2) major and minor DCs (Jost & Herrmann, 1989). Since the dominant DC components are mainly controlled by crustal stress condition and fault architecture (see section 4.1), the secondary components of the moment tensors likely reflect contributions from fault initiation by fluid involvement or complex/jogged fault structure. We consider the potential contributions from these two interpretations further.

First, it has been suggested that tensile cracks likely propagate along the S_H direction during hydraulic fracturing (Bell & Grasby, 2012). At the microseismic scale (i.e., $M < 0$), large non-DC components have been frequently documented and regarded as evidence for tensile-crack opening (Baig & Urbancic, 2010; Ross et al., 1996; Šílený et al., 2009; Šílený & Milev, 2008). A similar mechanism has been proposed for more sizable events ($-2 < M < 2$) in geothermal regions (e.g., Foulger & Long, 1984). Our moment tensor decomposition analysis suggests that similar physical processes may contribute to hydraulic-fracturing-induced events in the WCSB (Figure 3b). Both the resolved CLVD components and regional S_H orientations (Reiter et al., 2014) are aligned subparallel to the NE-SW direction, consistent with hydraulic fracture propagation during stage

stimulations. For earthquakes in the WCSB, the CLVD components (M2.1–3.8) are usually smaller than the DC components (M3.1–4.4; also see Figure 3) but above the microseismic range ($M < 0$). In fact, the estimated fracture opening for a crack with 300-m length would be a few centimeters (seismic potency P_0 ~0.1 km^{2}cm; Ben-Zion, 2008), which is capable of producing an M~3 non-DC event. Specific to the Duvernay, a 200-m length was used as an acceptable estimate for geomechanical modeling of fracture propagation (Lele et al., 2017) and ~1-cm fracture apertures are observed when higher-viscosity fluids are used (Maxwell et al., 2016 October). The chosen length dimension is at the high end of hydraulic fracturing cases, where fractures grow up to hundreds of meters in length (Davies et al., 2012; Wilson et al., 2018). In addition, the limited amounts of isotropic components are disproportional to the CLVD for purely tensile cracks. Therefore, the above explanation may only partially explain the consistent CLVD, specific to the anticipated shearing motion of ~3 cm on an ~1-km^2 fault in connection with an M~4 strike-slip event.

Alternatively, the minor DCs show consistent NW-SE aligned normal faults. In other words, minor faults could have slipped as a part of an extensional duplex connecting the dextral N-S (and subvertical) shear slips (see Figure 3b). The averaged magnitude difference between major and minor DCs is 0.8: assuming that both the major and connecting (minor) faults share similar rupture distances, this corresponds to a tenfold fault length difference (Hanks & Kanamori, 1979). A strike-slip fault system with transtensional flower structure has been supported by geological evidence (Berger & Davies, 1999; Wang et al., 2016), as well as by recent seismic imaging at the basement depth in the Fox Creek area (Chopra et al., 2017; Corlett et al., 2018; Eaton et al., 2018). It is highly possible for transtensional faults to develop within the limited zone between en echelon fault strands (Sylvester, 1988). For matured complex fault zones, the connecting segments usually contain both thrust and normal faults (depends on their orientations and develop history), which deviate from simplified textbook examples. Interestingly, these fault structures are often related to vertical fluid flow (Cox, 2016; Davies & Smith, 2006)—a condition required for induced seismicity.

In summary, the orientation of CLVD components for hydraulic-fracturing-induced earthquakes offers tangible evidence for either crack opening or co-slipping on a transtensional fault system (see Figure 3b). The former explanation is typically favored by microseismicity/geothermal induced events, while the latter mechanism is common for natural events under tectonic environments (Frohlich, 1994). Because induced earthquakes may be treated as a mix of these two classes of seismicity, we cannot rule out the possibility that both interpretations may be valid for the earthquakes in central Alberta.

4.3. The Non-DC Component: Prevalence and Implications

The non-DC components provide details on how fluid injection/extraction reactivates (more realistic) faults, with multiple physical explanations. However, improperly constrained non-DC components could lead to confounding reasoning or misinterpretation (Vavryčuk et al., 2008). Many factors including hypocentral location, station coverage, and velocity model may affect the resolution and amount of non-DC contributions. For example, a large non-DC may be introduced due to insufficient coverage during borehole monitoring (Eyre & van der Baan, 2017). Insufficient station coverage is particularly concerning for focal mechanism solutions of natural earthquakes in the WCSB, especially those before 2010. To mitigate undesired hypocentral and structural effects, we carefully compare and select input hypocenter locations from multiple sources and use industry-verified depths (see supporting information). We also examined the potential relationship between our observed amounts of non-DC in western Canada with earthquake depth and magnitude and found no clear relationships (Figure S29). This may be attributable to the variations in the amounts of non-DC components.

The statistics of decomposition of our collected data sets (see section 2.2) show comparable amounts of non-DC among six independent categories (Figure 4a). This result raises questions about the effectiveness of using non-DC as a reliable metric in identifying an induced event (e.g., Dahm et al., 2013; Zhang et al., 2016). On the one hand, we observe very limited (~3%) isotropic components from induced events in the WCSB, which differ greatly from fluid-induced earthquakes during geothermal (i.e., Martínez-Garzón et al., 2017) and mining-related (Cesca et al., 2013) activities. Figure 4b shows a 2-D Hudson's plot, which partitions a full moment tensor of an earthquake into DC, CLVD, and isotropic components (Hudson et al., 1989). Most of the induced events in the WCSB are located within the fourth quadrant of Hudson's plot, which corresponds to tensile-crack opening with a limited volume increase. In contrast, events located in Germany (mostly mining induced) are more randomly distributed in all four quadrants, showing greater isotropic components. Our results suggest that the volume changes during hydraulic fracturing are only responsible for an

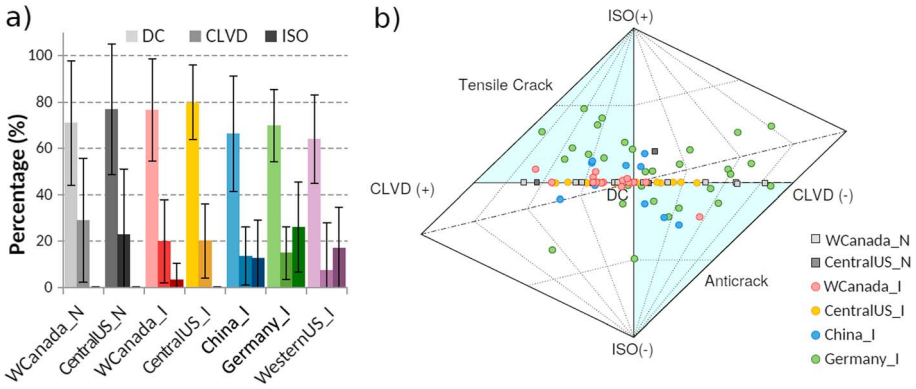

Figure 4. Decompositions of collected data set. (a) Averaged percentages (shaded bars) and standard deviations (black error bars) of the DC, CLVD, and isotropic components (ISO). (b) Hudson's plot summarizing the decomposed moment tensors for the listed regions. Geothermal induced events (purple bars) in the western United States are only presented in (a) (moment tensor values are unavailable). For both plots, tectonic events (labeled with "*N*") are shown in gray scale and induced events (labeled with "*I*") are shown in color.

isotropic component that is less than 10% of the total moment during an *M*3 earthquake (i.e., *M*2.4), a value considerably smaller than those previously proposed for events in the WCSB (Zhang et al., 2016). Natural and induced intraplate events in western Canada exhibit comparable amounts (29 versus 20% on average, respectively) as well as substantial variations (see Figure 4a) of CLVD. Large variations in the CLVD components are also observed for both types of earthquakes in central United States; unfortunately, their isotropic components have been preset to zero during moment tensor solutions (Global Centroid Moment Tensor solutions). Overall, due to the marginal differences among the various earthquake types, we suggest that the proper determination of the nature of an event (induced or natural) should rely more on the background seismicity and the spatiotemporal correlation to industry activities rather than its focal mechanism.

Given the apparent lack of distinction between non-DC components for natural and induced events, we further speculate on the implications for natural events. In western Canada, the intraplate events vary substantially in location and possibly also involve slippages on en echelon faults other than the major mapped faults. For example, nonplanar faulting systems are common for large-scale natural events with significant non-DC components, as evidenced by vertical CLVDs ("eyeballs") observed in volcanic regions (e.g., Minson et al., 2007; Shuler et al., 2013) and horizontal CLVDs ("baseballs") near mid-ocean ridges (e.g., Frohlich, 1994; Miller et al., 1998). Regardless of the nature of an earthquake, complex regional fault systems can produce CLVD components via similar mechanisms. Assisted by dynamic triggering stresses (Wang et al., 2015), the fluid-fault interaction (Cox, 2016) rationale can also be responsible for the slippages of critically stressed faults that produced natural earthquakes. For the isotopic component, mass perturbation due to injection/extraction does not ensure a larger volume change in each of related earthquake and therefore may be case specific (e.g., hydraulic-fracturing and volcanic earthquakes may contain lower isotropic components than previous suspected). Taken together, both the uncertainties and complex source physics can lead to the indistinguishable amounts of non-DC between natural and induced events at regional scales.

5. Conclusions

This paper presents our first and preliminary collection of focal mechanisms from several key regions with human-induced earthquakes (and their interpretations). Our integrated evaluation of recent intraplate earthquakes in western Canada, as well as several worldwide clusters, leads to the following conclusions:

The focal mechanisms of the induced earthquakes in the WCSB can be separated into strike-slip events within central Alberta and thrust faulting events along the Canadian Rockies—similar to tectonic earthquakes. Events in Fox Creek contain minimal isotropic components while sharing highly consistent CLVD components with *p* axis orientated along NE-SW. We interpreted this finding as a consequence of tensile-crack opening and/or en echelon faults co-slipping. Induced events in western Canada have comparable non-DC

components to those of natural and induced earthquakes elsewhere, leaving their focal mechanisms indistinguishable. This observation suggests that fluid-fault interactions or complex fault architectures play an important role in natural intraplate events too.

Acknowledgments
The authors thank John Ristau, Simone Cesca, and Xinlin Lei for sharing the moment values of some studied events. Most figures in this paper were generated using the Generic Mapping Tool (Wessel et al., 2013), and Figure 2a was made based on Matlab codes shared by Vaclav Vavryčuk. Moment values of analyzed events are presented in Table S1 in the supporting information. Earthquake catalogs and moment tenors in the United States are generated from USGS (United States Geological Survey) online catalog and GCMT (Global Centroid Moment Tensor Catalog). Lastly, we would like to thank Editor Gavin Hayes and two anonymous reviewers for their suggestions and critiques that helped improve the quality of this paper. This work was supported by the Natural Science and Engineering Research Council of Canada (NSERC) Discovery Grant.

References

Atkinson, G. M., Eaton, D. W., Ghofrani, H., Walker, D., Cheadle, B., Schultz, R., et al. (2016). Hydraulic fracturing and seismicity in the western Canada Sedimentary Basin. *Seismological Research Letters*, *87*(3), 631–647. https://doi.org/10.1785/0220150263

Babaie Mahani, A., Schultz, R., Kao, H., Walker, D., Johnson, J., & Salas, C. (2017). Bulletin of the Seismological Society of America (2017) *107*(2): 542–552. https://doi.org/10.1785/0120160175

Baig, A., & Urbancic, T. (2010). Microseismic moment tensors: A path to understanding frac growth. *The Leading Edge*, *29*(3), 320–324. https://doi.org/10.1190/1.3353729

Bao, X., & Eaton, D. W. (2016). Fault activation by hydraulic fracturing in western Canada. *Science*, *354*(6318), 1406–1409. https://doi.org/10.1126/science.aag2583

Bell, J. S., & Grasby, S. E. (2012). The stress regime of the western Canadian sedimentary basin. *Geofluids*, *12*(2), 150–165. https://doi.org/10.1111/j.1468-8123.2011.00349.x

Ben-Zion, Y. (2008). Collective behavior of earthquakes and faults: Continuum-discrete transitions, progressive evolutionary changes, and different dynamic regimes. *Reviews of Geophysics*, *46*, RG4006. https://doi.org/10.1029/2008RG000260

Berger, Z., & Davies, G. R. (1999). The development of linear hydrothermal dolomite (HTD) reservoir facies along wrench or strike slip fault systems in the western Canada Sedimentary Basin. *Canadian Society of Petroleum Geologists Reservoir*, *26*(1), 34–38.

Cesca, S., Rohr, A., & Dahm, T. (2013). Discrimination of induced seismicity by full moment tensor inversion and decomposition. *Journal of Seismology*, *17*(1), 147–163. https://doi.org/10.1007/s10950-012-9305-8

Chen, X., Nakata, N., Pennington, C., Haffener, J., Chang, J. C., He, X., et al. (2017). The Pawnee earthquake as a result of the interplay among injection, faults and foreshocks. *Scientific Reports*, *7*(1), 4945. https://doi.org/10.1038/s41598-017-04992-z

Chopra, S., Sharma, R. K., Ray, A. K., Nemati, H., Morin, R., Schulte, B., & D'Amico, D. (2017). Seismic reservoir characterization of Duvernay shale with quantitative interpretation and induced seismicity considerations—A case study. *Interpretation*, *5*(2), T185–T197. https://doi.org/10.1190/INT-2016-0130.1

Corlett, H., Schultz, R., Branscombe, P., Hauck, T., Haug, K., MacCormack, K., & Shipman, T. (2018). Subsurface faults inferred from reflection seismic, earthquakes, and sedimentological relationships: Implications for induced seismicity in Alberta, Canada. *Marine and Petroleum Geology*, *93*, 135–144. https://doi.org/10.1016/j.marpetgeo.2018.03.008

Cox, S. F. (2016). Injection-driven swarm seismicity and permeability enhancement: Implications for the dynamics of hydrothermal ore systems in high fluid-flux, overpressured faulting regimes—An invited paper. *Economic Geology*, *111*(3), 559–587. https://doi.org/10.2113/econgeo.111.3.559

Dahm, T., Becker, D., Bischoff, M., Cesca, S., Dost, B., Fritschen, R., et al. (2013). Recommendation for the discrimination of human-related and natural seismicity. *Journal of Seismology*, *17*(1), 197–202. https://doi.org/10.1007/s10950-012-9295-6

Davies, G. R., & Smith, L. B. Jr. (2006). Structurally controlled hydrothermal dolomite reservoir facies: An overview. *AAPG Bulletin*, *90*(11), 1641–1690. https://doi.org/10.1306/05220605164

Davies, R. J., Mathias, S. A., Moss, J., Hustoft, S., & Newport, L. (2012). Hydraulic fractures: How far can they go? *Marine and Petroleum Geology*, *37*(1), 1–6. https://doi.org/10.1016/j.marpetgeo.2012.04.001

Doglioni, C. (2017). A classification of induced seismicity. *Geoscience Frontiers*. ISSN 1674-9871. https://doi.org/10.1016/j.gsf.2017.11.015

Duggan, J. P., Mountjoy, E. W., & Stasiuk, L. D. (2001). Fault-controlled dolomitization at swan hills Simonette oil field (Devonian), deep basin west-Central Alberta, Canada. *Sedimentology*, *48*(2), 301–323. https://doi.org/10.1046/j.1365-3091.2001.00364.x

Dunn, L., Schmidt, G., Hammermaster, K., Brown, M., Bernard, R., Wen, E., et al. (2012). *The Duvernay Formation (Devonian): Sedimentology and Reservoir Characterization of a Shale Gas/Liquids Play in Alberta, Canada*. Calgary, Canada: Canadian Society of Petroleum Geologists, Annual Convention. Program with Abstracts, available at https://www.cspg.org/cspg/Conferences/Geoconvention/2012_Abstract_Archives.aspx

Earthquakes Canada (2018). Retrieved from http://csegrecorder.com/assets/pdfs/2014/2014-11-RECORDER-Basic_Geomechanics.pdf

Eaton, D. W., Igonin, N., Poulin, A., Weir, R., Zhang, H., Pellegrino, S., & Rodriguez, G. (2018). Induced seismicity characterization during hydraulic-fracture monitoring with a shallow-wellbore geophone array and broadband sensors. *Seismological Research Letters*, *89*, 1641–1651. https://doi.org/10.1785/0220180055

Efron, B., & Tibshirani, R. (1991). Statistical data analysis in the computer age. *Science*, *253*(5018), 390–395. https://doi.org/10.1126/science.253.5018.390

Ellis, R. M., Spence, G. D., Clowes, R. M., Waldron, D. A., Jones, I. F., Green, A. G., et al. (1983). The Vancouver Island seismic project: A co-CRUST onshore–offshore study of a convergent margin. *Canadian Journal of Earth Sciences*, *20*(5), 719–741. https://doi.org/10.1139/e83-065

Ellsworth, W. L. (2013). Injection-induced earthquakes. *Science*, *341*(6142). https://doi.org/10.1126/science.1225942

Evans, K. F., Zappone, A., Kraft, T., Deichmann, N., & Moia, F. (2012). A survey of the induced seismic responses to fluid injection in geothermal and CO_2 reservoirs in Europe. *Geothermics*, *41*, 30–54. https://doi.org/10.1016/j.geothermics.2011.08.002

Eyre, T. S., & van der Baan, M. (2017). The reliability of microseismic moment tensor solutions: Surface versus borehole monitoring. *Geophysics*, *82*(6), 1–46. https://doi.org/10.1190/geo2017-0056.1

Fischer, T., & Guest, A. (2011). Shear and tensile earthquakes caused by fluid injection. *Geophysical Research Letters*, *38*, L05307. https://doi.org/10.1029/2010GL045447

Foulger, G., & Long, R. E. (1984). Anomalous focal mechanisms: Tensile crack formation on an accreting plate boundary. *Nature*, *310*(5972), 43–45. https://doi.org/10.1038/310043a0

Foulger, G. R., Wilson, M., Gluyas, J., Julian, B. R., & Davies, R. (2018). Global review of human-induced earthquakes. *Earth-Science Reviews*, *178*, 438–514. https://doi.org/10.1016/j.earscirev.2017.07.008

Frohlich, C. (1994). Earthquakes with non-double-couple mechanisms. *Science*, *264*(5160), 804–809. https://doi.org/10.1126/science.264.5160.804

Ge, S., Liu, M., Lu, N., Godt, J. W., & Luo, G. (2009). Did the Zipingpu reservoir trigger the 2008 Wenchuan earthquake? *Geophysical Research Letters*, *36*, L20315. https://doi.org/10.1029/2009GL040349

Grigoli, F., Cesca, S., Priolo, E., Rinaldi, A. P., Clinton, J. F., Stabile, T. A., et al. (2017). Current challenges in monitoring, discrimination, and management of induced seismicity related to underground industrial activities: A European perspective. *Reviews of Geophysics*, *55*, 310–340. https://doi.org/10.1002/2016RG000542

Grigoli, F., Cesca, S., Rinaldi, A. P., Manconi, A., López-Comino, J. A., Clinton, J. F., et al. (2018). The November 2017 M_w 5.5 Pohang earthquake: A possible case of induced seismicity in South Korea. *Science*, *360*(6392), 1003–1006. https://doi.org/10.1126/science.aat2010

Gu, Y. J., Okeler, A., Shen, L., & Contenti, S. (2011). The Canadian Rockies and Alberta network (CRANE): New constraints on the Rockies and western Canada sedimentary basin. *Seismological Research Letters*, *82*(4), 575–588. https://doi.org/10.1785/gssrl.82.4.575

Guglielmi, Y., Cappa, F., Avouac, J. P., Henry, P., & Elsworth, D. (2015). Seismicity triggered by fluid injection-induced aseismic slip. *Science*, *348*(6240), 1224–1226. https://doi.org/10.1126/science.aab0476

Guilhem, A., Hutchings, L., Dreger, D. S., & Johnson, L. R. (2014). Moment tensor inversions of *M*~3 earthquakes in the geysers geothermal fields, California. *Journal of Geophysical Research: Solid Earth*, *119*, 2121–2137. https://doi.org/10.1002/2013JB010271

Hanks, T. C., & Kanamori, H. (1979). A moment magnitude scale. *Journal of Geophysical Research*, *84*(B5), 2348–2350. https://doi.org/10.1029/JB084iB05p02348

Heidbach, O., Rajabi, M., Reiter, K. Ziegler, M., & WSM Team (2016). World Stress Map database release 2016, GFZ Data Services. https://doi.org/10.5880/WSM.2016.001

Huang, Y., Ellsworth, W. L., & Beroza, G. C. (2017). Stress drops of induced and tectonic earthquakes in the Central United States are indistinguishable. *Science Advances*, *3*(8), e1700772. https://doi.org/10.1126/sciadv.1700772

Hudson, J. A., Pearce, R. G., & Rogers, R. M. (1989). Source type plot for inversion of the moment tensor. *Journal of Geophysical Research*, *94*(B1), 765–774. https://doi.org/10.1029/JB094iB01p00765

Johnson, K. L., Hayes, G. P., Herrmann, R. B., Benz, H. M., McNamara, D. E., & Bergman, E. (2016). RMT focal plane sensitivity to seismic network geometry and faulting style. *Geophysical Journal International*, *206*(1), 525–556. https://doi.org/10.1093/gji/ggw141

Jost, M. U., & Herrmann, R. B. (1989). A student's guide to and review of moment tensors. *Seismological Research Letters*, *60*(2), 37–57.

Kim, K. H., Ree, J. H., Kim, Y., Kim, S., Kang, S. Y., & Seo, W. (2018). Assessing whether the 2017 M_w 5.4 Pohang earthquake in South Korea was an induced event. *Science*, *360*(6392), 1007–1009. https://doi.org/10.1126/science.aat6081

Lei, X., Huang, D., Su, J., Jiang, G., Wang, X., Wang, H., et al. (2017). Fault reactivation and earthquakes with magnitudes of up to M_w4.7 induced by shale-gas hydraulic fracturing in Sichuan Basin, China. *Scientific Reports*, *7*(1), 7971. https://doi.org/10.1038/s41598-017-08557-y

Lei, X., Ma, S., Chen, W., Pang, C., Zeng, J., & Jiang, B. (2013). A detailed view of the injection-induced seismicity in a natural gas reservoir in Zigong, southwestern Sichuan Basin, China. *Journal of Geophysical Research: Solid Earth*, *118*, 4296–4311. https://doi.org/10.1002/jgrb.50310

Lele, S. P., Tyrrell, T., & Dasari, G. R. (2017). Geomechanical analysis of fault reactivation due to hydraulic fracturing. In *51st US Rock Mechanics/Geomechanics Symposium*. American Rock Mechanics Association. 25-28 June, San Francisco, CA, USA.

Martínez-Garzón, P., Kwiatek, G., Bohnhoff, M., & Dresen, G. (2017). Volumetric components in the earthquake source related to fluid injection and stress state. *Geophysical Research Letters*, *44*, 800–809. https://doi.org/10.1002/2016GL071963

Maxwell, S., Chorney, D., Smith, M., & Mack, M. (2016). Microseismic geomechanical interpretation of asymmetric hydraulic fractures. *SEG Technical Program Expanded Abstracts 2016* (pp. 2,569–2,573). Dallas, Texas: Society of Exploration Geophysicists. https://doi.org/10.1190/segam2016-13970147.1

McGarr, A., & Barbour, A. J. (2017). Wastewater disposal and the earthquake sequences during 2016 near Fairview, Pawnee, and Cushing, Oklahoma. *Geophysical Research Letters*, *44*, 9330–9336. https://doi.org/10.1002/2017GL075258

McGarr, A., Bekins, B., Burkardt, N., Dewey, J., Earle, P., Ellsworth, W., et al. (2015). Coping with earthquakes induced by fluid injection. *Science*, *347*(6224), 830–831. https://doi.org/10.1126/science.aaa0494

Mignan, A., Broccardo, M., Wiemer, S., & Giardini, D. (2017). Induced seismicity closed-form traffic light system for actuarial decision-making during deep fluid injections. *Scientific Reports*, *7*(1), 13607. https://doi.org/10.1038/s41598-017-13585-9

Miller, A. D., Foulger, G. R., & Julian, B. R. (1998). Non-double-couple earthquakes 2. Observations. *Reviews of Geophysics*, *36*(4), 551–568. https://doi.org/10.1029/98RG00717

Minson, S. E., Dreger, D. S., Bürgmann, R., Kanamori, H., & Larson, K. M. (2007). Seismically and geodetically determined nondouble-couple source mechanisms from the 2000 Miyakejima volcanic earthquake swarm. *Journal of Geophysical Research*, *112*, B10308. https://doi.org/10.1029/2006JB004847

Pakzad, M., Moradi, A., Afra, M., & Hosseini, H. (2018). Resolvability of moment tensors in Iran. *Geophysical Journal International*, *214*(1), 133–147. https://doi.org/10.1093/gji/ggy130

Petersen, M. D., Mueller, C. S., Moschetti, M. P., Hoover, S. M., Shumway, A. M., McNamara, D. E., et al. (2017). 2017 one-year seismic-hazard forecast for the central and eastern United States from induced and natural earthquakes. *Seismological Research Letters*, *88*(3), 772–783. https://doi.org/10.1785/0220170005

Reiter, K., Heidbach, O., Schmitt, D., Haug, K., Ziegler, M., & Moeck, I. (2014). A revised crustal stress orientation database for Canada. *Tectonophysics*, *636*, 111–124. https://doi.org/10.1016/j.tecto.2014.08.006

Ristau, J., Rogers, G. C., & Cassidy, J. F. (2007). Stress in western Canada from regional moment tensor analysis. *Canadian Journal of Earth Sciences*, *44*(2), 127–148. https://doi.org/10.1139/e06-057

Ross, A., Foulger, G. R., & Julian, B. R. (1996). Non-double-couple earthquake mechanisms at the geysers geothermal area, California. *Geophysical Research Letters*, *23*(8), 877–880. https://doi.org/10.1029/96GL00590

Schmitt, D. R. (2014). Basic geomechanics for induced seismicity: A tutorial. *CSEG Recorder (Nov 2014)*, *39*(11), 20–27. Retrieved from https://csegrecorder.com/articles/view/the-regional-alberta-observatory-for-earthquake-studies-network-raven

Schoenball, M., Walsh, F. R., Weingarten, M., & Ellsworth, W. L. (2018). How faults wake up: The Guthrie-Langston, Oklahoma earthquakes. *The Leading Edge*, *37*(2), 100–106. https://doi.org/10.1190/tle37020100.1

Schultz, R., Atkinson, G., Eaton, D. W., Gu, Y. J., & Kao, H. (2018). Hydraulic fracturing volume is associated with induced earthquake productivity in the Duvernay play. *Science*, *359*(6373), 304–308. https://doi.org/10.1126/science.aao0159

Schultz, R., Corlett, H., Haug, K., Kocon, K., MacCormack, K., Stern, V., & Shipman, T. (2016). Linking fossil reefs with earthquakes: Geologic insight to where induced seismicity occurs in Alberta. *Geophysical Research Letters*, *43*, 2534–2542. https://doi.org/10.1002/2015GL067514

Schultz, R., Mei, S., Pană, D., Stern, V., Gu, Y. J., Kim, A., & Eaton, D. (2015). The Cardston earthquake swarm and hydraulic fracturing of the Exshaw formation (Alberta Bakken play). *Bulletin of the Seismological Society of America*, *105*(6), 2871–2884. https://doi.org/10.1785/0120150131

Schultz, R., & Stern, V. (2015). The regional Alberta Observatory for Earthquake Studies Network (RAVEN). *CSEG Recorder*, *40*(8), 34–37.

Schultz, R., Stern, V., & Gu, Y. J. (2014). An investigation of seismicity clustered near the Cordel field, west-Central Alberta, and its relation to a nearby disposal well. *Journal of Geophysical Research: Solid Earth*, *119*, 3410–3423. https://doi.org/10.1002/2013JB010836

Schultz, R., Wang, R., Gu, Y. J., Haug, K., & Atkinson, G. (2017). A seismological overview of the induced earthquakes in the Duvernay play near Fox Creek, Alberta. *Journal of Geophysical Research: Solid Earth*, *122*, 492–505. https://doi.org/10.1002/2016JB013570

Shuler, A., Ekström, G., & Nettles, M. (2013). Physical mechanisms for vertical-CLVD earthquakes at active volcanoes. *Journal of Geophysical Research: Solid Earth*, *118*, 1569–1586. https://doi.org/10.1002/jgrb.50131

Šílený, J. (2009). Resolution of non-double-couple mechanisms: Simulation of hypocenter mislocation and velocity structure mismodeling. *Bulletin of the Seismological Society of America*, *99*(4), 2265–2272. https://doi.org/10.1785/0120080335

Šílený, J., Hill, D. P., Eisner, L., & Cornet, F. H. (2009). Non-double-couple mechanisms of microearthquakes induced by hydraulic fracturing. *Journal of Geophysical Research*, *114*, B08307. https://doi.org/10.1029/2008JB005987

Šílený, J., & Milev, A. (2008). Source mechanism of mining induced seismic events—Resolution of double couple and nondouble couple models. *Tectonophysics*, *456*(1-2), 3–15. https://doi.org/10.1016/j.tecto.2006.09.021

Sylvester, A. G. (1988). Strike-slip faults. *Geological Society of America Bulletin*, *100*(11), 1666–1703. https://doi.org/10.1130/0016-7606(1988)100<1666:SSF>2.3.CO;2

Tao, W., Masterlark, T., Shen, Z. K., & Ronchin, E. (2015). Impoundment of the Zipingpu reservoir and triggering of the 2008 M_w 7.9 Wenchuan earthquake, China. *Journal of Geophysical Research: Solid Earth*, *120*, 7033–7047. https://doi.org/10.1002/2014JB011766

van der Baan, M., & Calixto, F. J. (2017). Human-induced seismicity and large-scale hydrocarbon production in the USA and Canada. *Geochemistry, Geophysics, Geosystems*, *18*, 2467–2485. https://doi.org/10.1002/2017GC006915

Vavryčuk, V., Bohnhoff, M., Jechumtálová, Z., Kolář, P., & Šílený, J. (2008). Non-double-couple mechanisms of microearthquakes induced during the 2000 injection experiment at the KTB site, Germany: A result of tensile faulting or anisotropy of a rock? *Tectonophysics*, *456*(1-2), 74–93. https://doi.org/10.1016/j.tecto.2007.08.019

Wang, B., Harrington, R. M., Liu, Y., Yu, H., Carey, A., & Elst, N. J. (2015). Isolated cases of remote dynamic triggering in Canada detected using cataloged earthquakes combined with a matched-filter approach. *Geophysical Research Letters*, *42*, 5187–5196. https://doi.org/10.1002/2015GL064377

Wang, R., Gu, Y. J., Schultz, R., Kim, A., & Atkinson, G. (2016). Source analysis of a potential hydraulic-fracturing-induced earthquake near Fox Creek, Alberta. *Geophysical Research Letters*, *43*, 564–573. https://doi.org/10.1002/2015GL066917

Wang, R., Gu, Y. J., Schultz, R., Zhang, M., & Kim, A. (2017). Source characteristics and geological implications of the January 2016 induced earthquake swarm near crooked Lake, Alberta. *Geophysical Journal International*, *210*(2), 979–988. https://doi.org/10.1093/gji/ggx204

Wessel, P., Smith, W. H. F., Scharroo, R., Luis, J. F., & Wobbe, F. (2013). Generic mapping tools: Improved version released. *EOS Transactions AGU*, *94*, 409–410. https://doi.org/10.1002/2013EO450001

Wilson, M. P., Foulger, G. R., Gluyas, J. G., Davies, R. J., & Julian, B. R. (2017). HiQuake: The human-induced earthquake database. *Seismological Research Letters*, *88*(6), 1560–1565. https://doi.org/10.1785/0220170112

Wilson, M. P., Worrall, F., Davies, R. J., & Almond, S. (2018). Fracking: How far from faults? *Geomechanics and Geophysics for Geo-Energy and Geo-Resources*, *4*(2), 193–199. https://doi.org/10.1007/s40948-018-0081-y

Zhang, H., Eaton, D. W., Li, G., Liu, Y., & Harrington, R. M. (2016). Discriminating induced seismicity from natural earthquakes using moment tensors and source spectra. *Journal of Geophysical Research: Solid Earth*, *121*, 972–993. https://doi.org/10.1002/2015JB012603

Zhang, Y., Person, M., Rupp, J., Ellett, K., Celia, M. A., Gable, C. W., et al. (2013). Hydrogeologic controls on induced seismicity in crystalline basement rocks due to fluid injection into basal reservoirs. *Groundwater*, *51*(4), 525–538. https://doi.org/10.1111/gwat.12071

Zhao, P., Kühn, D., Oye, V., & Cesca, S. (2014). Evidence for tensile faulting deduced from full waveform moment tensor inversion during the stimulation of the base enhanced geothermal system. *Geothermics*, *52*, 74–83. https://doi.org/10.1016/j.geothermics.2014.01.003